Transport study of graphene adsorbed with indium adatoms

Zhenzhao Jia, Baoming Yan, Jingjing Niu, Qi Han, Rui Zhu, Dapeng Yu, and Xiaosong Wu*
State Key Laboratory for Artificial Microstructure and Mesoscopic Physics, Peking University, Beijing 100871, China
and Collaborative Innovation Center of Quantum Matter, Beijing 100871, China
(Received 17 September 2014; revised manuscript received 7 November 2014; published 12 February 2015)

Enhancement of the spin-orbit coupling in graphene may lead to various topological phenomena and also find applications in spintronics. Adatom adsorption has been proposed as an effective way to achieve the goal. In particular, great hope has been held for indium in strengthening the spin-orbit coupling and realizing the quantum spin Hall effect. To search for evidence of the spin-orbit coupling in graphene adsorbed with indium adatoms, we carry out extensive transport measurements. It is found that indium adatoms dope graphene and introduce significant Coulomb scattering. No signature of the spin-orbit coupling is observed in the weak localization magnetoconductance and nonlocal spin Hall effect. Possible explanations are discussed.

DOI: 10.1103/PhysRevB.91.085411 PACS number(s): 72.25.Rb, 72.80.Vp, 73.43.−f, 81.05.ue

I. INTRODUCTION

The intrinsic spin-orbit coupling (SOC) in graphene is extremely weak [1–3]. Enhancement of the coupling may give rise to a variety of topological phenomena, such as the quantum spin Hall effect (two-dimensional topological insulators) [4–10], quantum anomalous Hall effect [11–16], and Chern half metals [17]. These phenomena are among the hottest topics in condensed matter physics. It is also predicted that Rashba SOC can add another π to the Berry phase [18] and lead to a new variety of unconventional quantum Hall effect (QHE) [19]. Moreover, graphene endowed with strong SOC can have potential use in spintronics, as SOC provides a means to control the spin electrically, which is at the heart of spintronics.

Adsorption of adatoms has been theoretically proposed as an effective way to enhance SOC in graphene [6–17,20–27]. By distorting the carbon sp^2 bond [20,22], breaking the inversion symmetry [6,11,22], or mediating the hopping between the second-nearest neighbors [4,6], intrinsic, or Rashba SOC can be enhanced or induced. The intrinsic SOC is required for the predicted quantum spin Hall effect, whereas Rashba SOC destroys it [4]. It has been proposed that if the outer shell electrons of adatoms derive from p orbitals, the induced intrinsic SOC always dominates over the induced Rashba interaction. Under this condition, it is possible to realize two-dimensional (2D) topological insulators in graphene [6]. The most promising candidates are indium and thallium, which can open up a significant topologically nontrivial gap. Further theoretical work has confirmed that the two systems are indeed stable topological insulators [8,9].

Two experimental groups have reported angle-resolved photoemission studies on the spin-orbit splitting in a related system, graphene on metal substrates [28–31]. Graphene on gold displays a very strong Rashba effect. On the other hand, it has been found that the spin relaxation rate measured by nonlocal spin valves is not enhanced by gold adatoms [32], suggesting SOC is negligible. Recently, a strong SOC has been observed in hydrogenated graphene and chemical vapor deposited graphene by the spin Hall effect (SHE) [33–35]. Nevertheless, in sharp contrast to numerous theoretical work on this topic, relevant experimental results, especially transport experiments, are scarce. This is in part due to two issues. One is related to the low diffusion barrier for metal adatoms [36], which causes clustering of adatoms at room temperature. The other is oxidation of adatoms.

In this work, we employ an ultra low-temperature magneto-transport measurement system, with *in situ* thermal deposition capability, to circumvent the two aforementioned issues. We choose indium, as it is reckoned by a few theoretical works as an ideal candidate [6,8,9]. Weak localization (WL) and nonlocal SHE measurements have been carried out for different indium coverages with the aim of searching for evidence of SOC. Comparison with relevant theories has been made and no transport signature of SOC has been observed. We discuss the possible reasons for absence of transport signature, which shed light on future studies.

II. EXPERIMENT

Graphene flakes were exfoliated from Kish graphite onto 285-nm SiO_2/Si substrates. Standard e-beam lithography and metallization processes were used to make Hall bar structures. Electrodes are made of 5-nm Pd/ 80-nm Au. Samples were annealed in Ar/H_2 atmosphere at 260 °C for 2 hours to remove photoresist and other chemical residues and then transferred into our dilution refrigerator. The system is a modified Oxford dilution refrigerator, in which *in situ* thermal deposition can be performed [37]. Before the first deposition, current annealing was done to remove gas adsorption. The current density was 0.2 mA/μm [38]. During deposition and measurements, the sample temperature was maintained below 5 K, much less than the diffusion barrier for indium on graphene [39]. Thus the adatom diffusion and clustering were strongly suppressed. Electrical measurements were done by a standard low-frequency lock-in technique.

The sample geometry can be seen in the scanning electron microscopy image in Fig. 1(a). The half-integer QHE is well developed, which confirms that the sample is monolayer graphene. The low-field magnetoresistivity is plotted in Fig. 1(b). The narrow negative magnetoresistivity peak at $B = 0$ is WL, while the noiselike but reproducible fluctuations are universal conductance fluctuations. Weak localization is caused by constructive interference of electrons along time

*xswu@pku.edu.cn

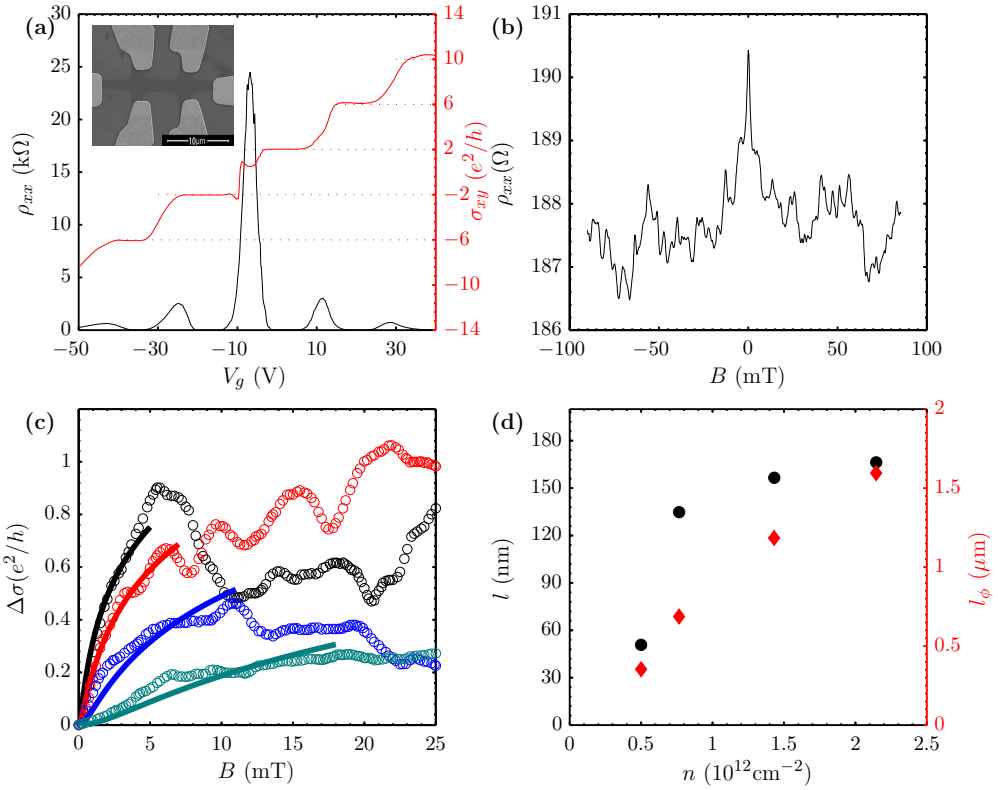

FIG. 1. (Color online) Magnetotransport of a graphene Hall bar device before indium deposition. (a) Longitudinal resistivity and the transverse conductivity vs the gate voltage in 9 T at 150 mK. The inset is a scanning electron microscopy picture of the device. (b) Low-field magnetoresistivity exhibits two features, the weak localization peak at $B = 0$ and the universal conductance fluctuations. (c) Fits to Eq. (1) for the low-field magnetoconductivity at different carrier densities, $n = 2.15, 1.43, 0.77, 0.50 \times 10^{12}$ cm^{-2}. (d) The mean free path l and the phase coherence length l_ϕ as a function of n_s.

reversal paths. In graphene, electrons are chiral and have a Berry phase π, which inverts the constructive interference to a destructive one. Thus intrinsic graphene should display weak antilocalization (WAL). However, in the presence of intervalley scattering, resulting from short-range potential, there will be a crossover from suppressed WL to WAL as the field increases [40–43]. The high-field behavior, e.g., the crossover field, is determined by intervalley and intravalley scatterings, while the low-field part is governed by the phase coherence time and not affected by the former two scattering times (see Fig. S1 in Ref. [44]). When the intervalley scattering rate exceeds the phase coherence rate, the low-field WL correction to the conductivity can be expressed as [45]

$$\Delta\sigma = -\frac{e^2}{2\pi h}\left[F\left(\frac{B}{B_\phi}\right) - F\left(\frac{B}{B_\phi + 2B_{\rm asy}}\right) - 2F\left(\frac{B}{B_\phi + B_{\rm asy} + B_{\rm sym}}\right)\right], \quad (1)$$

$$F(z) = \ln z + \psi\left(\frac{1}{2} + \frac{1}{z}\right), B_{\phi,{\rm asy},{\rm sym}} = \frac{\hbar}{4De\tau_{\phi,{\rm asy},{\rm sym}}},$$

where ψ is the digamma function, e the elementary charge and $\hbar$ the reduced Planck constant. D is the diffusion constant and τ_ϕ is the phase coherence time. $\tau_{\rm asy}$, $\tau_{\rm sym}$ are the $z \to -z$ asymmetric and symmetric spin-orbit scattering time, respectively. For pristine graphene, SOC is negligible. Then, Eq. (1) reproduces the low-field results of Ref. [40]. To establish the baseline for later comparison, we have measured WL at different gate voltages (carrier densities), shown in Fig. 1(c). Data are fitted to Eq. (1) with only one parameter τ_ϕ while setting $B_{\rm asy}$ and $B_{\rm asy}$ to zero. To meet the low-field requirement of Eq. (1) and also avoid the influence of the universal conductance fluctuations, only the low-field positive magnetoconductance are fitted. A good agreement with the theory is found. The mean free path l is calculated from the resistivity and carrier density. Considering the charge puddles in graphene, the carrier density at the Dirac point is taken as 0.5×10^{12} cm^{-2} [46]. l and the phase coherence length l_ϕ are plotted in Fig. 1(d). l_ϕ decreases as one approaches the Dirac point. This is because τ_ϕ in graphene is determined by electron-electron interaction, which is enhanced when screening is weakened. The suppression of τ_ϕ is further enhanced by the reduction of the mean free time τ [47].

III. RESULTS AND DISCUSSION

Indium deposition was performed *in situ* at a very slow rate for several times, each lasting 22–300 seconds. During deposition, the sample resistance was monitored so that a desired shift of the Dirac point could be obtained. After each deposition, electrical measurements were carried out. The conductivity σ as a function of gate voltage is plotted in Fig. 2(a). The Dirac point gradually shifts to negative gate

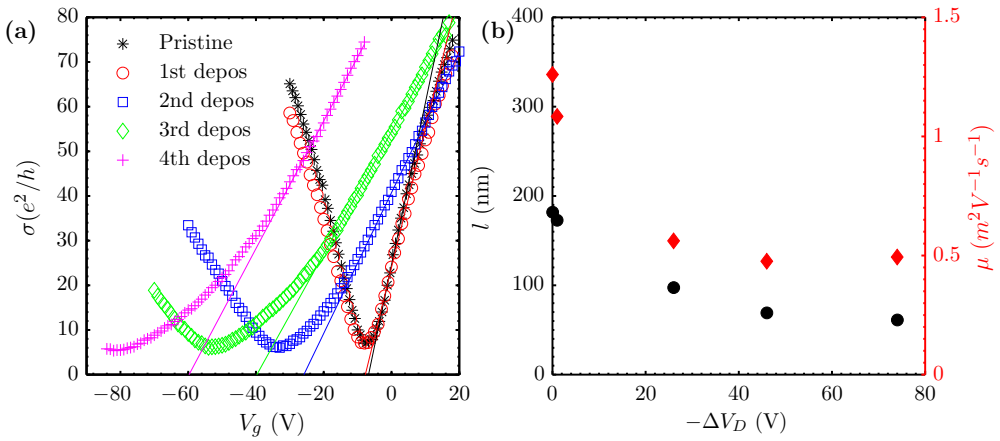

FIG. 2. (Color online) Deposition of indium. (a) The conductivity σ vs gate voltage V_g curves for the device after each deposition. The solid lines are linear fits, from which the field effect mobility is obtained. (b) The dependence of the mean free path l and mobility μ on the shift of the Dirac point $\Delta V_{\rm D}$.

voltage as the indium coverage increases, indicating electron doping. At the same time, the conductivity turns from sublinear to linear in $V_{\rm g}$. The linear dependence is attributed to charged impurity scattering being dominant [46]. So, the transition to the linear dependence suggests that indium adatoms mainly introduce charged impurities (long-range potential), rather than short-range potential. The minimum conductivity $\sigma_{\rm min}$ at the Dirac point remains relatively constant, about $6e^2/h$, while a closer look shows a slight decrease with increasing adatom density. A similar dependence of $\sigma_{\rm min}$ has also been observed in potassium adsorbed graphene [48]. According to a self-consistent theory proposed by Adams *et al.* [46], $\sigma_{\rm min}$ is a consequence of two competing effects of charged impurities. One is to scatter electrons. The other is to generate a residue carrier density at the Dirac point by doping. The result is a weak negative dependence of $\sigma_{\rm min}$ on the impurity density. At the same, the width of the $\sigma_{\rm min}$ plateau increases, which is observed in our experiment. So, all features in the density dependence of the conductivity are consistent with charged impurity scattering. Its implication on SOC will be discussed later.

We now estimate the area density of indium adatoms $n_{\rm In}$. Assume that each indium adatom transfers Z electrons to graphene. If adatoms are dilute, Z should be a constant [46]. Then, the doped carrier density $\overline{n} = Zn_{\rm In}$. $\overline{n}$ can be estimated from the shift of the Dirac point $\Delta V_{\rm D}$, as $\overline{n} = c_{\rm g}\Delta V_{\rm D}/e$. Here, $c_{\rm g}$ is the gate capacitance for 285-nm SiO_2 dielectric. The only uncertainty is the value of Z. According to first-principles calculations, Z for indium on graphene is $0.8 \sim 1$ [6,36,39]. To get an idea of the coverage, we adopt $Z = 1$ to obtain its lower bound. Consequently, the area density after the third deposition is 3.1×10^{12} cm^{-2}, corresponding to a coverage of 0.25%. The average spacing between adatoms is 18 nm, which is already much shorter than the mean free path before deposition, suggesting that scattering is dominated by adatoms.

From the gate dependence of the conductivity, the field effect mobility μ is obtained. Its dependence on $\Delta V_{\rm D}$, which is proportional to $n_{\rm In}$, is plotted in Fig. 2(b), as well the mean free path l at a carrier density of 3.8×10^{12} cm^{-2}. As the mobility is substantially reduced after deposition, it is evident that adatom scattering dominates. We now look for signature of SOC induced by adatoms. WAL has been employed as a sensitive probe for SOC [49,50]. In conventional 2D electron gases with absence of SOC, the magnetoconductance is positive, the hallmark of WL, stemming from constructive interference of electrons along time reversal paths. When SOC is turned on, it rotates the electron spin and produces destructive interference, giving rise to WAL, a negative magnetoconductance. W(A)L can be seen as a time-of-flight experiment. Specifically, interactions of a longer time scale manifest themselves in a lower magnetic field [51]. So, as SOC increases, WAL first emerges from zero field and eventually dictates the whole field regime. The conductance correction is given by the HLN equation [49]:

$$\Delta\sigma(B) = -g_s g_v \frac{e^2}{\pi h}\left[\psi\left(\frac{1}{2}+\frac{B_1}{B}\right) - \psi\left(\frac{1}{2}+\frac{B_2}{B}\right) + \frac{1}{2}\psi\left(\frac{1}{2}+\frac{B_3}{B}\right) - \frac{1}{2}\psi\left(\frac{1}{2}+\frac{B_4}{B}\right)\right], \quad (2)$$

where

$$B_1 = B_0 + B_{\rm so} + B_{\rm s},$$
$$B_2 = \frac{4}{3}B_{\rm so} + \frac{2}{3}B_{\rm s} + B_\phi,$$
$$B_3 = 2B_{\rm s} + B_\phi,$$
$$B_4 = \frac{2}{3}B_{\rm s} + \frac{4}{3}B_{\rm so} + B_\phi.$$

Here, $B_0 = \hbar/4De\tau$ and $B_{{\rm so,s},\phi} = \hbar/4De\tau_{{\rm so,s},\phi}$. $\tau_{\rm so}$ and $\tau_{\rm s}$ represent spin-orbit scattering time and magnetic scattering time, respectively. Although defects in graphene has been reported to introduce magnetic scattering, it is neglected in the following analysis as the scattering time ($\approx$200 ps) is much long than the phase coherence time of our sample [52].

In graphene, the expected evolution of magnetoconductance with increasing SOC is qualitatively similar. The reason is that, although intrinsic graphene display WAL, opposite to conventional 2D electron gases, typical graphene films show

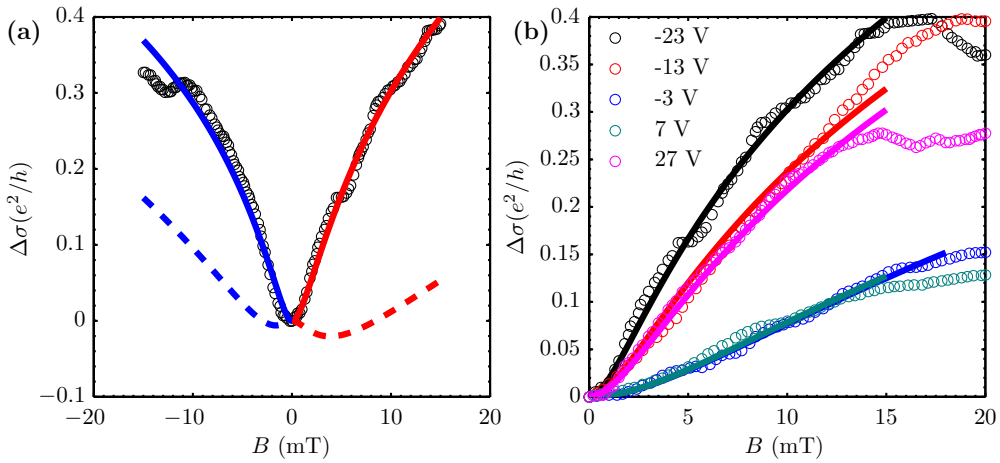

FIG. 3. (Color online) Low-field magnetoconductivity after the third deposition. (a) Fits of the low-field magnetoconductivity to Eqs. (1) and (2). The circles are experimental data. The solid lines are the best fits to the equations, red for Eq. (1) and blue for Eq. (2). The dotted lines are plots of two equations, assuming a spin-orbit scattering time $\tau_{so} = \tau_\phi$. (b) Magnetoconductivity data and fits to Eq. (1) at different gate voltages relative to the Dirac point ($V_g - V_D$).

WL due to presence of defects. From the theory in Ref. [45], the magnetoconductance correction in low field is given by Eq. (1) [45]. Compared with conventional 2D electron gases, the effect of SOC on WL depends on symmetry. For $z \to -z$ asymmetric SOC, normal crossover from WL to WAL occurs, while for $z \to -z$ symmetric SOC, WL will be suppressed. For adatom adsorbed graphene, if any induced SOC, the $z \to -z$ asymmetric component should be substantial [45]. It is anticipated that the magnetoconductance goes from negative to positive as the magnetic field increases. Therefore both conventional 2D electron gases and graphene are predicted to show similar nonmonotonic magnetoconductance, which can be readily recognized without any fitting. This is the feature that we are particularly interested in.

Figure 3(a) shows the low-field magnetoconductance after the third deposition. The magnetoconductance monotonically increases with field, except for universal conductance fluctuations. No trace of WAL near $B = 0$ has been found. Fitting of the data to Eq. (1) yields $\tau_\phi = 8.6$ ps, while τ_{asy} and τ_{sym} are an order of magnitude larger than τ_ϕ with significant standard deviations, which essentially suggests inappreciable SOC. We have also performed fitting to Eq. (2). The obtained τ_ϕ is similar, $\approx$10.9 ps. Again, τ_{so} is much larger than τ_ϕ, consistent with Eq. (1). To illustrate the expected influence of SOC, both equations are plotted with τ_ϕ obtained by fitting and all spin-orbit scattering time being equal to τ_ϕ. The resultant nonmonotonic magnetoconductance is distinct from the experiment data. In fact, extensive measurements of the magnetoconductance at various carrier densities and after each deposition have been carried out and none of them shows WAL around $B = 0$ (see Ref. [44]).

Since τ_ϕ can be seen as a cutoff time for the quantum interference, it is reasonable to estimate that τ_{so} is longer than τ_ϕ at least. Assume Elliott-Yafet spin-orbit scattering, $\tau_{so} = (E_F/\Delta_{so})^2\tau$ [53]. The upper-bound of the spin-orbit coupling strength Δ_{so} is then estimated as 12 meV at a carrier density of 1.67×10^{12} cm^{-2}. We emphasize that this is the local SOC strength during scattering of electrons off an adatom, but not the overall spin-orbit gap of 7 meV at a 6% coverage calculated in Ref. [6]. In the theory, the spin-orbit splitting on an indium adatom is on the order of 100 meV. The upper bound obtained in our experiment is actually much smaller than the prediction.

As a comparison, we have also performed the same experiments with *in situ* deposition of magnesium. Magnesium is a light element. It introduces little spin-orbit coupling (SOC) [54]. If indium can significantly enhances the SOC, the magnetotransport should be qualitatively different from magnesium.

Magnetoresistance of pristine graphene before Mg deposition is shown in Fig. 4. The field effect mobility is 11400 cm^2/Vs. The sample exhibits the half-integer quantum Hall effect, confirming that it is a monolayer. The low-field resistance displays a weak localization peak around $B = 0$ and universal conductance fluctuations. By fitting the weak localization peak to Eq. (1), the carrier density dependence of the phase coherence length l_ϕ is obtained and plotted in Fig. 4(d), as well as the mean free path l.

Upon Mg deposition, the Dirac point shifts towards negative gate voltage due to electron doping, see Fig. 5. At the same time, the density dependence of σ turns linear, indicating dominance of long-range scatterers. This observation is consistent with In deposition. As these metal adatoms electron-dope graphene by charge transfer, they are positive charged. Scattering by these ionized adatoms is dictated by the long-range Coulomb potential, instead of the short-range component. This is in accordance with previous studies in which noticeable short-range scattering occurs for insulating neutral adsorbates [55,56].

The low-field magnetoconductivity after deposition is shown in Fig. 6(a). It remains positive, as expected for negligible SOC. Equations (1) and (2) are used to fit the data. The fit to Eq. (1) yields $\tau_\phi = 18.5$ ps, while the fit to Eq. (2) gives a similar value $\tau_\phi = 20.6$ ps. In both cases, the fitted τ_{so} is much larger than τ_ϕ. The expected nonmonotonic magnetoconductivity with increasing field for $\tau_{so} = \tau_\phi$ is plotted in Fig. 6(a), in contrast to the monotonic behavior of

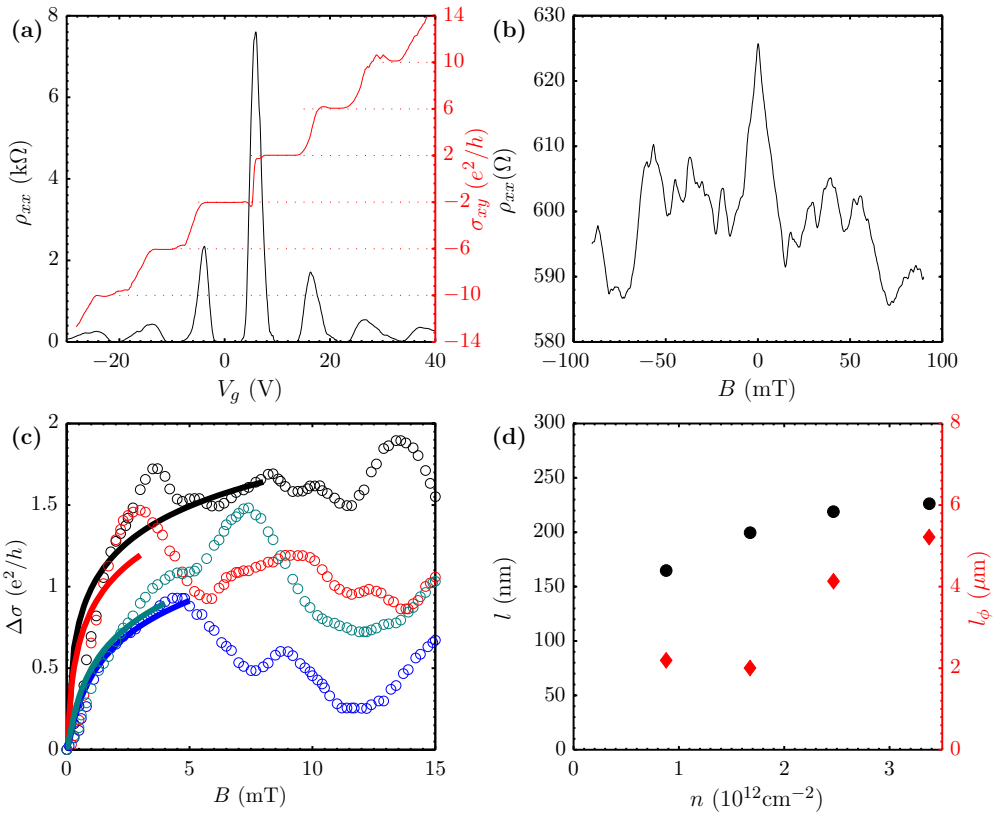

FIG. 4. (Color online) Magnetotransport of a graphene Hall bar device before Mg deposition. (a) Longitudinal resistivity and the transverse conductivity vs the gate voltage in 9 T at 150 mK, showing the half-integer quantum Hall effect. (b) Low-field magnetoresistivity exhibits two features, the weak localization peak at $B = 0$ and the universal conductance fluctuations. (c) Fits to Eq. (1) for the low-field magnetoconductivity at different carrier densities. (d) The mean free path l and the phase coherence length l_ϕ as a function of n_s. l_ϕ is obtained from the fits in (c).

the experimental curve. The qualitatively same WL behavior for In and Mg deposition confirms that no appreciable SOC is induced by indium.

Another effect that may arise because of SOC is SHE. In a spin-orbit coupled system, a charge current generates a spin transport in the transverse direction, called SHE, and vice versa, called reverse SHE. The cooperation of two effects leads to a nonlocal resistance [57], $R_{\mathrm{nl}} = \frac{1}{2}(\frac{\beta_s}{\sigma})^2 \frac{W}{\sigma l_s} e^{-L/l_s}$, where β_s is the spin Hall conductivity, l_s is the spin diffusion length, L and W are the length and width of the sample, respectively. This effect can be used to detect SOC. A large SOC in hydrogenated graphene and chemical vapor deposited graphene has been experimentally confirmed by this method

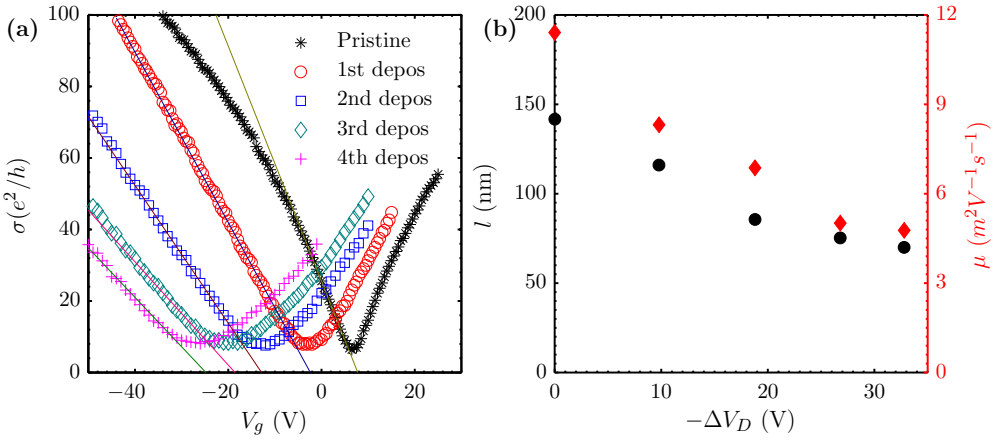

FIG. 5. (Color online) Deposition of magnesium. (a) The conductivity σ vs gate voltage V_g curves for the device after each deposition. The solid lines are linear fits, from which the field effect mobility is obtained. (b) The dependence of the mean free time τ at a carrier density of 1.7×10^{12} cm^2/Vs and the field effect mobility μ on the shift of the Dirac point ΔV_{D}.

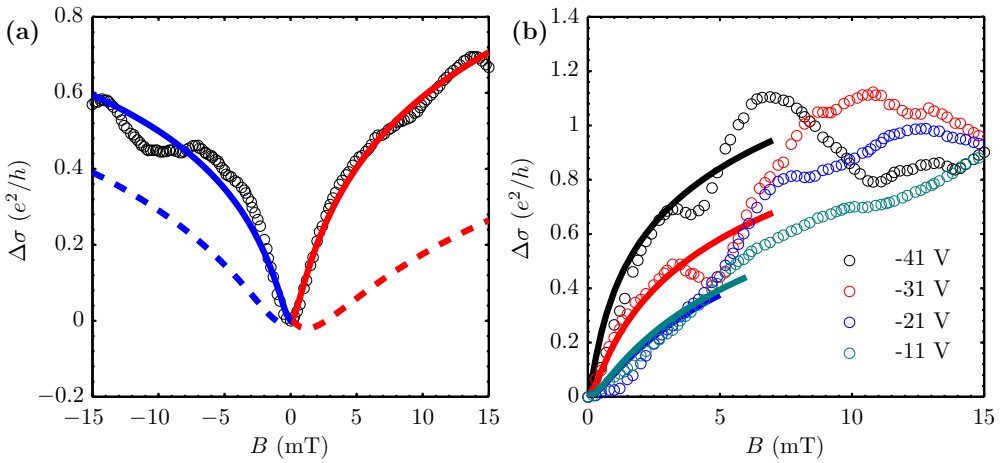

FIG. 6. (Color online) Low-field magnetoconductivity after the fourth deposition of Mg. (a) Fit of the low-field magnetoconductivity at a carrier density of 1.7×10^{12} cm^2/Vs to Eq. (1) and Eq. (2). The circles are experimental data. The solid lines are the best fits to the equations, red for Eq. (1) and blue for Eq. (2). The dotted lines are plots of two equations, assuming a spin-orbit scattering time $\tau_{so} = \tau_\phi$. (b) Magnetoconductivity data and fits to Eq. (1) at different gate voltages relative to the Dirac point. The fluctuations of the conductivity are reproducible and due to universal conductance fluctuations.

[33–35]. Here, we have measured the nonlocal resistance by injecting current through one pair of Hall probes of the Hall bar while monitoring the voltage signal across the other pair of Hall probes. The nonlocal resistance as a function of the gate voltage before and after deposition is plotted in Fig. 7(b). There is 0.6 Ω nonlocal resistance before deposition. The amplitude of the resistance is consistent with the Ohmic contribution, which decays as $e^{-\pi L/W}$. After deposition, no substantial change has been observed, indication of no appreciable induced SOC. Taking 0.6 Ω as the upper bound of the nonlocal resistance due to SHE and $\beta_s/\sigma \approx 0.45$ at a carrier density of 1×10^{12} cm^2/Vs from Ref. [33] for hydrogenated graphene, we estimate $\tau_{so} = 37$ ps, i.e., $\Delta_{so} = 1.3$ meV. This is an order of magnitude smaller than the 12 meV upper-bound estimated by WL. It should be pointed out that the estimation here is crude in that β_s/σ is apparently a function of the SOC and unlikely the same as hydrogenated graphene.

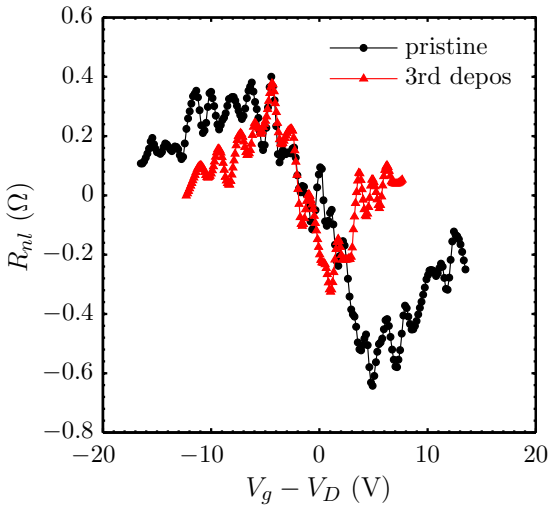

FIG. 7. (Color online) Nonlocal SHE measurements. The nonlocal signal is very weak, on a level comparable to noise. No substantial change occurs after indium deposition.

Whereas the theories have listed indium as an important candidate for enhancing SOC in graphene and realizing a 2D topological insulator, we fail to find any signature of SOC by transport measurements. It is noteworthy that the potential of adatoms has been theoretically treated as a short-range one, as SOC is induced by mediating the hopping between the first, second, and third nearest neighbors [27]. However, the carrier density dependence of the conductivity does not support considerable increase of short-range scattering upon deposition. Similar observations have been made for magnesium and potassium [48]. The absence of transport signature of induced SOC may be associated with dominant long-range Coulomb potential of ionized adatoms. We notice that a recent study has shown that titanium particles dope graphene and give rise to long-range scattering. However, when these particles are oxidized, charge transfer is reduced, indicated by the doping level. At the same time, significant short-range scattering appears [56]. This implies that long-range potential could "screen" short-range potential. Manifestation of SOC in the weak localization and spin Hall effect relies on spin-orbit scattering, rather than an overall spin-orbit splitting of the band structure. So, both effects probe the local SOC during scattering of electrons off adatoms. In the presence of a strong long-range potential, electrons will have less chance to get close enough to experience the SOC near the adatom, which will reduce its strength probed by transport. This may explain the discrepancy between the transport results of gold adsorbed graphene and the angle resolved photoemission spectroscopy of graphene on Au/Ni substrates [30–32]. Another possibility is that the bond between indium adatoms and graphene is van der Waals in nature. The interaction is too weak to modify the hopping between neighbours. Further study may focus on elements that induce less charge transfer, such as Fe or can form a stronger bond to graphene.

IV. CONCLUSION

By employing *in situ* evaporation, we have systematically studied the effect of indium adatom adsorption on the low-temperature electrical transport of graphene. The carrier density dependence of the conductivity reveals that indium adatoms act as long-range Coulomb scattering centers. The low-field magnetoconductance exhibits weak localization behavior at different carrier densities and indium coverages. Absence of weak antilocalization suggests negligible spin-orbit scattering. Experiments on magnesium adsorption, which will not introduce significant spin-orbit scattering, have also been carried out. The electrical transport is qualitatively the same, confirming no spin-orbit scattering induced by indium. Nonlocal measurements yield no appreciable spin Hall effect, corroborating with the magnetotransport studies.

ACKNOWLEDGMENTS

This work was supported by National Key Basic Research Program of China (Nos. 2012CB933404 and 2013CBA01603) and NSFC (Project Nos. 11074007, 11222436, and 11234001). X. W. thanks P. Xiong for providing details of his *in situ* deposition design.

[1] D. Huertas-Hernando, F. Guinea, and A. Brataas, Phys. Rev. B **74**, 155426 (2006).
[2] H. Min, J. E. Hill, N. A. Sinitsyn, B. R. Sahu, L. Kleinman, and A. H. MacDonald, Phys. Rev. B **74**, 165310 (2006).
[3] Y. G. Yao, F. Ye, X. L. Qi, S. C. Zhang, and Z. Fang, Phys. Rev. B **75**, 041401 (2007).
[4] C. L. Kane and E. J. Mele, Phys. Rev. Lett. **95**, 226801 (2005).
[5] C. L. Kane and E. J. Mele, Phys. Rev. Lett. **95**, 146802 (2005).
[6] C. Weeks, J. Hu, J. Alicea, M. Franz, and R. Wu, Phys. Rev. X **1**, 021001 (2011).
[7] J. Hu, J. Alicea, R. Wu, and M. Franz, Phys. Rev. Lett. **109**, 266801 (2012).
[8] H. Jiang, Z. Qiao, H. Liu, J. Shi, and Q. Niu, Phys. Rev. Lett. **109**, 116803 (2012).
[9] O. Shevtsov, P. Carmier, C. Groth, X. Waintal, and D. Carpentier, Phys. Rev. B **85**, 245441 (2012).
[10] A. Cresti, D. Van Tuan, D. Soriano, A. W. Cummings, and S. Roche, Phys. Rev. Lett. **113**, 246603 (2014).
[11] Z. H. Qiao, S. Y. A. Yang, W. X. Feng, W. K. Tse, J. Ding, Y. G. Yao, J. Wang, and Q. Niu, Phys. Rev. B **82**, 161414 (2010).
[12] J. Ding, Z. Qiao, W. Feng, Y. Yao, and Q. Niu, Phys. Rev. B **84**, 195444 (2011).
[13] W.-K. Tse, Z. Qiao, Y. Yao, A. H. MacDonald, and Q. Niu, Phys. Rev. B **83**, 155447 (2011).
[14] Z. Qiao, H. Jiang, X. Li, Y. Yao, and Q. Niu, Phys. Rev. B **85**, 115439 (2012).
[15] H. Zhang, C. Lazo, S. Blügel, S. Heinze, and Y. Mokrousov, Phys. Rev. Lett. **108**, 056802 (2012).
[16] Z. Qiao, X. Li, W.-K. Tse, H. Jiang, Y. Yao, and Q. Niu, Phys. Rev. B **87**, 125405 (2013).
[17] J. Hu, Z. Zhu, and R. Wu, arXiv:1401.5453.
[18] X. Zhai and G. Jin, Phys. Rev. B **89**, 085430 (2014).
[19] E. I. Rashba, Phys. Rev. B **79**, 161409 (2009).
[20] A. H. Castro Neto and F. Guinea, Phys. Rev. Lett. **103**, 026804 (2009).
[21] K.-H. Ding, Z.-G. Zhu, and J. Berakdar, Europhys. Lett. **88**, 58001 (2009).
[22] S. Abdelouahed, A. Ernst, J. Henk, I. V. Maznichenko, and I. Mertig, Phys. Rev. B **82**, 125424 (2010).
[23] A. Dyrdał and J. Barnaś, Phys. Rev. B **86**, 161401 (2012).
[24] D. Ma, Z. Li, and Z. Yang, Carbon **50**, 297 (2012).
[25] M. Gmitra, D. Kochan, and J. Fabian, Phys. Rev. Lett. **110**, 246602 (2013).
[26] A. Ferreira, T. G. Rappoport, M. A. Cazalilla, and A. H. Castro Neto, Phys. Rev. Lett. **112**, 066601 (2014).
[27] A. Pachoud, A. Ferreira, B. Özyilmaz, and A. H. Castro Neto, Phys. Rev. B **90**, 035444 (2014).
[28] A. Varykhalov, J. Sánchez-Barriga, A. M. Shikin, C. Biswas, E. Vescovo, A. Rybkin, D. Marchenko, and O. Rader, Phys. Rev. Lett. **101**, 157601 (2008).
[29] Y. S. Dedkov, M. Fonin, U. Rüdiger, and C. Laubschat, Phys. Rev. Lett. **100**, 107602 (2008).
[30] O. Rader, A. Varykhalov, J. Sánchez-Barriga, D. Marchenko, A. Rybkin, and A. M. Shikin, Phys. Rev. Lett. **102**, 057602 (2009).
[31] D. Marchenko, A. Varykhalov, M. Scholz, G. Bihlmayer, E. Rashba, A. Rybkin, A. Shikin, and O. Rader, Nat Commun **3**, 1232 (2012).
[32] K. Pi, W. Han, K. M. McCreary, A. G. Swartz, Y. Li, and R. K. Kawakami, Phys. Rev. Lett. **104**, 187201 (2010).
[33] J. Balakrishnan, G. Kok Wai Koon, M. Jaiswal, A. H. Castro Neto, and B. Ozyilmaz, Nat. Phys. **9**, 284 (2013).
[34] J. Balakrishnan, G. K. W. Koon, A. Avsar, Y. Ho, J. H. Lee, M. Jaiswal, S.-J. Baeck, J.-H. Ahn, A. Ferreira, M. A. Cazalilla *et al.*, Nat. Commun. **5**, 4748 (2014).
[35] A. Avsar, J. Y. Tan, T. Taychatanapat, J. Balakrishnan, G. Koon, Y. Yeo, J. Lahiri, A. Carvalho, A. S. Rodin, E. O'farrell *et al.*, Nat. Commun. **5**, 4875 (2014).
[36] K. T. Chan, J. B. Neaton, and M. L. Cohen, Phys. Rev. B **77**, 235430 (2008).
[37] J. S. Parker, D. E. Read, A. Kumar, and P. Xiong, Europhys. Lett. **75**, 950 (2006).
[38] There is a possibility that gold might electromigrate onto graphene. If so, the density of gold particles should be extremely low, because the resistance of the graphene films *decreased* by about 1%, indicating negligible scattering by gold particles. Moreover, Ref. [31] has shown that gold particles do not introduce spin-orbit scattering.
[39] F. J. Ribeiro, J. B. Neaton, S. G. Louie, and M. L. Cohen, Phys. Rev. B **72**, 075302 (2005).
[40] E. McCann, K. Kechedzhi, V. I. Fal'ko, H. Suzuura, T. Ando, and B. L. Altshuler, Phys. Rev. Lett. **97**, 146805 (2006).
[41] X. S. Wu, X. B. Li, Z. M. Song, C. Berger, and W. A. de Heer, Phys. Rev. Lett. **98**, 136801 (2007).
[42] F. V. Tikhonenko, D. W. Horsell, R. V. Gorbachev, and A. K. Savchenko, Phys. Rev. Lett. **100**, 056802 (2008).
[43] A. M. R. Baker, J. A. Alexander-Webber, T. Altebaeumer, T. J. B. M. Janssen, A. Tzalenchuk, S. Lara-Avila, S. Kubatkin,

R. Yakimova, C.-T. Lin, L.-J. Li *et al.*, Phys. Rev. B **86**, 235441 (2012).
[44] See Supplemental Material at http://link.aps.org/supplemental/10.1103/PhysRevB.91.085411 for detailed illustration of weak localization in graphene and more low-field magnetoresistance data.
[45] E. McCann and V. I. Fal'ko, Phys. Rev. Lett. **108**, 166606 (2012).
[46] S. Adam, E. H. Hwang, V. M. Galitski, and S. Das Sarma, Proc. Natl. Acad. Sci. USA **104**, 18392 (2007).
[47] E. Abrahams, P. W. Anderson, P. A. Lee, and T. V. Ramakrishnan, Phys. Rev. B **24**, 6783 (1981).
[48] J. H. Chen, C. Jang, S. Adam, M. S. Fuhrer, E. D. Williams, and M. Ishigami, Nat. Phys. **4**, 377 (2008).
[49] S. Hikami, A. I. Larkin, and Y. Nagaoka, Prog. Theor. Phys. **63**, 707 (1980).
[50] G. Bergmann, Phys. Rev. Lett. **48**, 1046 (1982).
[51] G. Bergmann, Physics Reports **107**, 1 (1984).
[52] M. B. Lundeberg, R. Yang, J. Renard, and J. A. Folk, Phys. Rev. Lett. **110**, 156601 (2013).
[53] H. Ochoa, A. H. Castro Neto, and F. Guinea, Phys. Rev. Lett. **108**, 206808 (2012).
[54] A. G. Swartz, J.-R. Chen, K. M. McCreary, P. M. Odenthal, W. Han, and R. K. Kawakami, Phys. Rev. B **87**, 075455 (2013).
[55] W. Zhu, D. Neumayer, V. Perebeinos, and P. Avouris, Nano Lett. **10**, 3572 (2010).
[56] K. M. McCreary, K. Pi, and R. K. Kawakami, Appl. Phys. Lett. **98**, 192101 (2011).
[57] D. A. Abanin, R. V. Gorbachev, K. S. Novoselov, A. K. Geim, and L. S. Levitov, Phys. Rev. Lett. **107**, 096601 (2011).